energies

MDPI

Article

Effects of Oxygen Concentration on Soot Formation in Ethylene and Ethane Fuel Laminar Diffusion Flames

Hongling Ju [1], Renjie Zhou [1], Deman Zhang [2,*], Peng Deng [2,*] and Zhaowen Wang [3]

[1] Hubei Key Laboratory of Advanced Technology for Automotive Components, Wuhan University of Technology, Wuhan 430070, China
[2] Wuhan Second Ship Design and Research Institute, Wuhan 430205, China
[3] School of Energy and Power Engineering, Huazhong University of Science and Technology, Wuhan 430074, China
* Correspondence: deman134@sohu.com (D.Z.); dpeng85@sohu.com (P.D.)

Abstract: In studying the effects of oxygen concentration and molecular structure on the morphologies of the soot particles produced by hydrocarbon fuels, ethylene and ethane were chosen as experimental fuels. With a Gülde laminar coaxial diffusion flame device, a soot particle device was used to sample soot particles at different oxygen concentrations (21%, 24%, 26%, 28%, and 31%) and at different heights above a burner (HABs = 10 mm, 20 mm, 30 mm, 40 mm, and 50 mm). High-resolution transmission electron microscopy (HRTEM) was used to scrutinize and analyze the soot particles at varying oxygen concentrations. The findings suggest that at the same oxygen concentration, ethylene produces brighter and taller flames. With an increase in the oxygen concentration, ethylene flames and ethane flames gradually decrease in height and become brighter. With an increase in the HAB, the average primary soot particle diameter (D_p) increases initially and then decreases, the fractal dimension (D_f) increases, and the aggregates transition from strips and chains to clusters. At the same flame height (HAB = 30 mm), the D_p decreases, the D_f increases, the carbon layer torsion resistance (T_f) and the carbon layer spacing (D_s) increase, and the carbon layer changes from a parallel arrangement to a curved arrangement to form denser network aggregations.

Keywords: oxygen concentration; ethylene; ethane; morphology; nanostructure

Citation: Ju, H.; Zhou, R.; Zhang, D.; Deng, P.; Wang, Z. Effects of Oxygen Concentration on Soot Formation in Ethylene and Ethane Fuel Laminar Diffusion Flames. *Energies* **2024**, *17*, 3866. https://doi.org/10.3390/en17163866

Academic Editor: Pedro J. Coelho

Received: 11 July 2024
Revised: 3 August 2024
Accepted: 4 August 2024
Published: 6 August 2024

Introduction

The combustion of hydrocarbon fuels generates soot particles, which serve as a primary contributor to both air pollution and the greenhouse effect. To mitigate these kinds of emissions, it is imperative for the energy industry to urgently address the pressing need for efficient and cleaner combustion methodologies [1,2]. In order to lessen our reliance on fossil fuels, significant advancements have been made in the exploration of efficient and environmentally friendly alternative renewable fuels [3,4]. By employing laminar flame burners as a research tool, researchers are able to eliminate the extraneous variables present in the complex combustion processes found in internal combustion engines, gas turbines, and other equipment. This approach enables exclusive focus on the physical and chemical transformations that occur during the generation of soot [5].

Soot particle formation is a complex phenomenon involving gas-phase chemical reactions and particle dynamics [6]. The detailed process of soot particle formation encompasses the generation of gas-phase precursors, soot nucleation, particle surface growth, particle coalescence and agglomeration, and soot oxidation as well as fragmentation [7]. During the combustion of macromolecular fuels, small hydrocarbon molecules such as methane, ethane, and ethylene are produced, from which polycyclic aromatic hydrocarbons (PAHs) are formed through cyclization reactions and HACA (hydrogen abstraction and acetylene addition) mechanisms [8]. PAHs are generally considered precursors to soot particle formation and play a crucial role in determining the morphology of soot particles [8].

Previous studies have demonstrated that macromolecular fuels undergo pyrolysis, resulting in the formation of small molecular components, such as C_2H_4, C_3H_6, CH_4, C_2H_6, and C_3H_8, during combustion [9–11]; however, an increase in the oxygen concentration of fuel leads to an elevation in the concentration of soot precursors [12,13]. The presence of C_2 molecules is commonly acknowledged as crucial for soot particle formation [8]; therefore, investigating small-molecule fuels, particularly those containing C_2 compounds, is essential for understanding the mechanisms underlying soot generation processes.

In recent years, extensive research has been conducted on certain light hydrocarbons, such as methane [14,15], ethane [16], and ethylene [17–19], as potential alternative fuels. For example, the morphology of soot particles in flames has been investigated using a laminar diffusion flame test bench, thermal electrophoresis sampling, and high-resolution transmission electron microscopy (HRTEM), with their growth process explored. Hydrocarbon methane, which is the most basic hydrocarbon in nature, produces soot particles characterized by an exceptionally low fractal dimension no greater than 1.4 [14]. Other hydrocarbons produce soot particles with fractal dimensions greater than those of methane [16,17]. Therefore, the soot characteristics of laminar flames are affected by many factors, such as pressure, mixing, the oxygen concentration, etc.

Pressure plays a crucial role in both soot formation and oxidation. An increase in pressure enhances the chemical reaction within the flame, stimulates the growth of soot particles, increases both the average particle size and the rotation radius of primary soot particles, and enhances their degree of graphitization, maturity, and oxidation [15,16]. Mixing different fuels also significantly impacts the morphology and nanostructure of the soot particles generated; whether the fuels added contain carbon is a key point for discussion. When adding non-carbon fuels such as ammonia [18] or hydrogen [19] into the fuel mixture, the carbon content is reduced, thereby inhibiting the formation of soot particles and decreasing soot emissions. When adding carbon fuels, such as a hydrocarbon [17,18], to another hydrocarbon, the morphology of soot particles is closely related to the fuels' properties and the fuel mixing ratio. Non-carbon fuels and carbon-containing fuels have been employed simultaneously in many studies; for instance, hydrogen and methane were introduced into ethylene to investigate the impact of the mixing ratio of blended fuels on soot morphology [19].

As the primary oxidizer in fuel combustion, oxygen plays a crucial role in accelerating soot particle oxidation, thereby influencing their characteristics. The formation of soot particles in flames occurs rapidly (with soot aggregates being able to form within tens of milliseconds) and early in the combustion process [20]. If soot particles make complete contact with an oxidant after their formation, an exothermic oxidative reaction occurs, ultimately resulting in oxidation into H_2O and CO_2; if the oxygen-to-carbon ratio is insufficient, the combustion becomes inadequate, and the particles aggregate into larger chain structures [21]. Oh et al. [22], Chunpeng et al. [23], Escudero et al. [24], and Marek et al. [25] have all discussed the effects of oxygen concentration on the properties of soot particles.

Although the soot generation process exhibits similarities in ethylene and ethane flames, there are notable differences in the morphologies and nanostructures of the resulting soot particles; therefore, in this study, differences in the morphology and nanostructure of soot particles are analyzed from the perspective of the fuel's structure (C-C and C=C), and the morphology and nanostructure of soot particles in ethylene and ethane laminar flames are analyzed at various oxygen concentrations.

1. Experimental Description

1.1. The Experimental Device

This study utilized a Gülde laminar coaxial diffusion flame device, as illustrated in Figure 1. The experimental setup primarily consisted of a laminar flame burner, an air compressor, an air tank, an oxygen tank, a fuel gas tank, mass flowmeters, a high-speed camera, a computer system, and a soot particle sampling device. The laminar flow flame burner consisted of an inner tube, with a diameter of 12.7 mm, and an outer tube, with a

diameter of 88.9 mm. The height of the laminar flow flame burner was 179 mm. The fuel was delivered to the burner via the inner tube, while air entered through the annular space between the inner and outer tubes. The air inlet was equipped with a layer of glass balls and two layers of porous metal foam. Prior to entering the burner under the mass flowmeters' control, both the fuel and air had to undergo depressurization using a pressure-reduction valve. Fuel was introduced into the burner through duct 1, located at the bottom of the burner, while air was supplied through duct 2, positioned on its side. The soot particle sampling device was equipped with an adjustable base that facilitated sampling at different flame heights. The system comprised a motor, a controller, a probe, and an ultra-thin carbon film. The carbon film was securely attached to the probe, enabling automatic adsorption of the soot particles on the basis of thermophoresis. Furthermore, a high-speed camera was employed to capture variations in the flame structure at different oxygen concentrations.

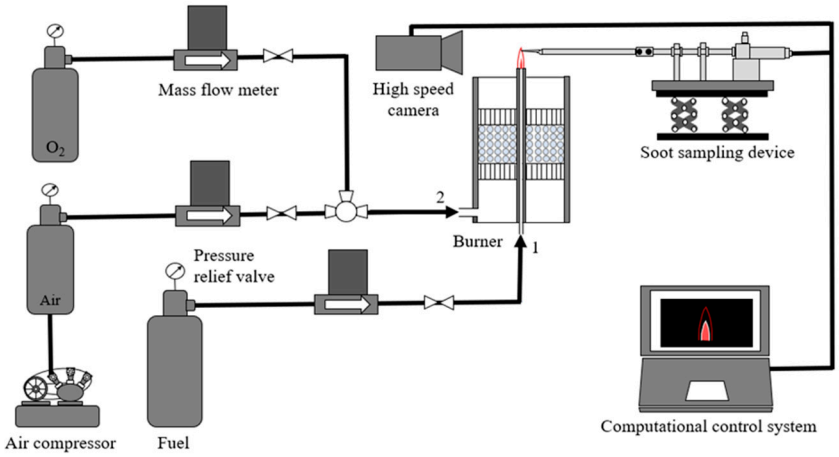

Figure 1. Schematic of the Gülde laminar coaxial diffusion flame device.

1.2. Experimental Conditions

During the experiment, the total airflow and oxygen flow rate were maintained at a constant value of 160 L/min, while the fuel flow rate was fixed at 0.15 L/min. The oxygen concentration in the laminar flame was adjusted by regulating the airflow and oxygen flow rates. Five different cases were investigated, with corresponding oxygen concentrations of 21%, 24%, 26%, 28%, and 31%, as presented in Table 1. The fuels used in this experiment include ethylene and ethane.

Table 1. The experimental conditions.

Case	Oxygen Concentration (%)	Air Flow Rate (L/min)	Oxygen Flow Rate (L/min)	Fuel Flow Rate (L/min)
1	21	160	0	0.15
2	24	153.9	6.1	0.15
3	26	149.9	10.1	0.15
4	28	145.8	14.2	0.15
5	31	139.7	20.3	0.15

1.3. Sample Methods

The sampling device was utilized to precisely adjust the tweezers and position the carbon film parallel to the flame axis. Based on the findings of Katsufumi et al. [26], sampling at the four locations depicted in Figure 2 not only minimized potential biases caused by the observation positions within the statistical results but also ensured that an adequate number of samples were obtained to meet the statistical requirements. The number of primary soot particle samples was between 600 and 1000 at each measurement location.

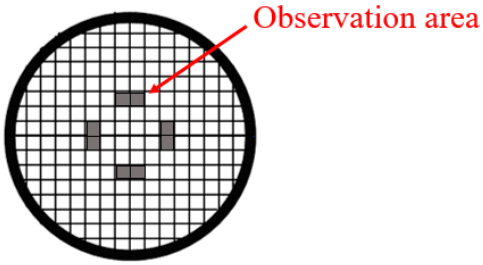

Figure 2. Detection positions on the carbon film.

While the copper network is at risk of burning if the sampling duration is excessively long, too brief a sampling period may yield an insufficient number of samples. After conducting numerous experiments and tests, it was determined that a sampling time of 25 milliseconds was optimal.

The time interval between sampling soot particles and conducting a TEM observation should be strictly controlled to within 24 h in order to preserve the original morphology of the soot particles to the maximum extent possible. Furthermore, each parameter of the soot particles was measured and statistically analyzed by the same person in order to minimize the potential for human error.

In this study, the sampling height was adjusted by controlling the base of the sampling device. Samples were collected at intervals of 10 mm along the flame axis, specifically at the distances of 10 mm, 20 mm, 30 mm, 40 mm, and 50 mm from the combustion port.

The agglomeration of the soot particles was analyzed following the methods of A.M. Brasil [27], Jiangjun Wei [28], and Tengfei Wang [29]. Fractal parameters of the soot particles, such as the fractal dimension (D_f), the primary soot particle diameter (D), the average primary soot particle diameter (D_p), the carbon layer torsion resistance (T_f), and the carbon layer spacing (D_s), were calculated.

2. The Effects of Oxygen Concentration on the Structure of Ethylene and Ethane Flames

Figure 3 illustrates the flame structure of the ethylene and ethane laminar diffusion flames at varying oxygen concentrations. Both the ethylene and ethane flames exhibited a consistent trend, with a gradual decrease in the flame height being observed as the oxygen concentration increased. Specifically, the heights of the ethylene flames were successively measured to be 64 mm, 57 mm, 50 mm, 45 mm, and 39 mm, while the heights of the ethane flames were successively measured to be 52 mm, 47 mm, 41 mm, 38 mm, and 35 mm. Consequently, under identical oxygen concentrations, it can be inferred that ethylene flames are taller and brighter. Considering the equivalent camera resolution parameters used to capture the images in this study, it can be speculated that a more intense brightness corresponds to a higher flame temperature [30].

At an oxygen concentration of 31%, the ethylene flames exhibited bifurcation at the top, while no such phenomenon was observed for the ethane flames. The reason for this is that the combustion reaction is more intense as the oxygen concentration increases, promoting soot particle growth and increasing the particle concentration [31]. When the soot particles ascend higher up the flame and are not completely oxidized, they escape from the top of the flame and break through the smooth flame to form a "flame wing"; however, a "flame wing" is potentially not observed in the ethane flame due to its width. The wider the flame, the greater the volume fraction of soot particles contained in the flame per unit time, and as the soot particles reside in the flame for longer, their oxidation is prolonged and more complete [31].

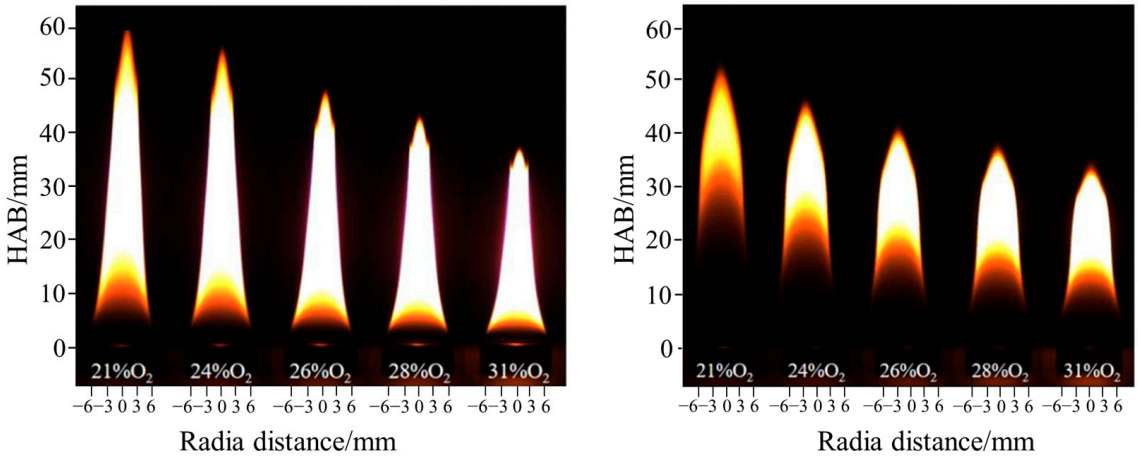

Figure 3. Evolution of the flame shape, height, and lightness with increasing oxygen concentrations.

3. Analysis of Soot Particle Morphologies at the Same Oxygen Concentration

3.1. Flame Structure and Soot Particle Morphologies

Figure 4 shows the flame structures for ethylene and ethane at an oxygen concentration of 21%. As this figure shows, the ethylene flame is significantly taller than the ethane flame, at 64.34 mm and 52.11 mm, respectively. This makes the ethylene flame 12.23 mm taller than the ethane flame. The ethylene flame is bright white, while the ethane flame is orange-yellow, consistent with the observations of David et al. [32]. These differences are caused by the presence of C=C double bonds in ethylene, which are unsaturated bonds that break easily during combustion, resulting in a high rate of heat release from ethylene [33]. In addition, the densest soot particle generation occurs in the brightest central region of the flame, and the thermal radiation generated by an abundance of soot particles also leads to an increase in the brightness of the flame [34].

The soot particle morphologies In the ethylene and ethane flames were observed at different heights above the burner using an HRTEM (JEOL company, Tokyo, Japan) at an oxygen concentration of 21%. The images of the soot particles were magnified 50,000 times, as shown in Figure 4.

The shaded region at the lowest flame height (height above the burner (HAB) = 10 mm) mainly consists of the gas-phase chemical reaction zone and the soot nucleation zone, where liquid soot particles and translucent soot particle agglomerates are visible on the carbon film. At an HAB = 20 mm, the small soot particles continue to collide and agglomerate, resulting in the soot particles partially overlapping and generating straight- chain-like agglomerates with a larger particle size and a darker base color. The brightest area of the flame is seen at an HAB = 30 mm, where the temperature is the highest and the soot particle concentration is the greatest. Here, the soot particle agglomerates gradually change from straight chains to ring-like structures, and the overlap of the agglomerates increases. At an HAB = 40 mm/50 mm, the flame becomes narrow, and the gas flow rate accelerates, which increases the chances of soot particles colliding and aggregating, thus strengthening their agglomeration, leading to increased primary soot particle aggregation and forming larger soot particles. The soot particle morphologies gradually change from ring-like to a dense, fibrous mesh structure. As shown in Figure 4, with an increase in the flame height, the soot particle generation process is divided into four stages: the gas-phase precursor, soot nucleation, particle coalescence and agglomeration, and oxidation, which is consistent with the results of many previous studies [35,36].

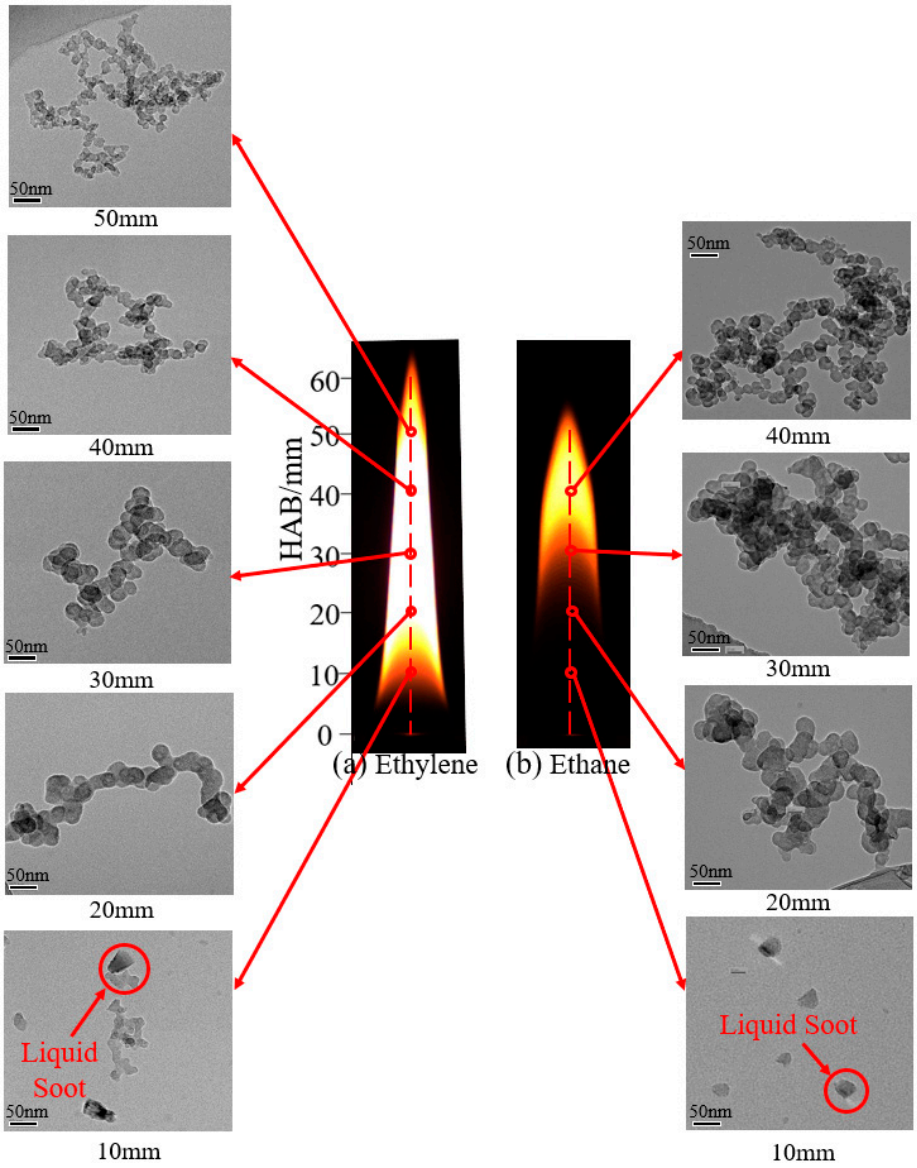

Figure 4. Change in soot particle morphologies of ethylene and ethane with flame heights at an oxygen concentration of 21%.

3.2. The Fractal Dimensions of the Soot Particles

Figure 5 shows *D* at different heights for the ethylene and ethane flames. In both the ethylene and ethane flames, *D* is predominantly distributed in the range of 5~55 nm. The results indicate that *D* of the ethylene and ethane increases and then decreases with an increase in flame height, in agreement with the findings of Chu [17]. This phenomenon can be attributed to the complex physicochemical processes within the flames. At lower flame heights (HAB = 10–20 mm), primary soot particles are formed, resulting in smaller particle sizes and smaller D distribution intervals. As the flame rises (HAB = 20–30 mm), the primary soot particles experience surface growth, causing the primary soot particles to gradually become mature, with larger particle sizes and the widest distribution interval. As the flame height increases further (HAB = 40–50 mm), oxygen diffusion is enhanced, and the oxidation results in smaller particle sizes and narrower D distribution intervals.

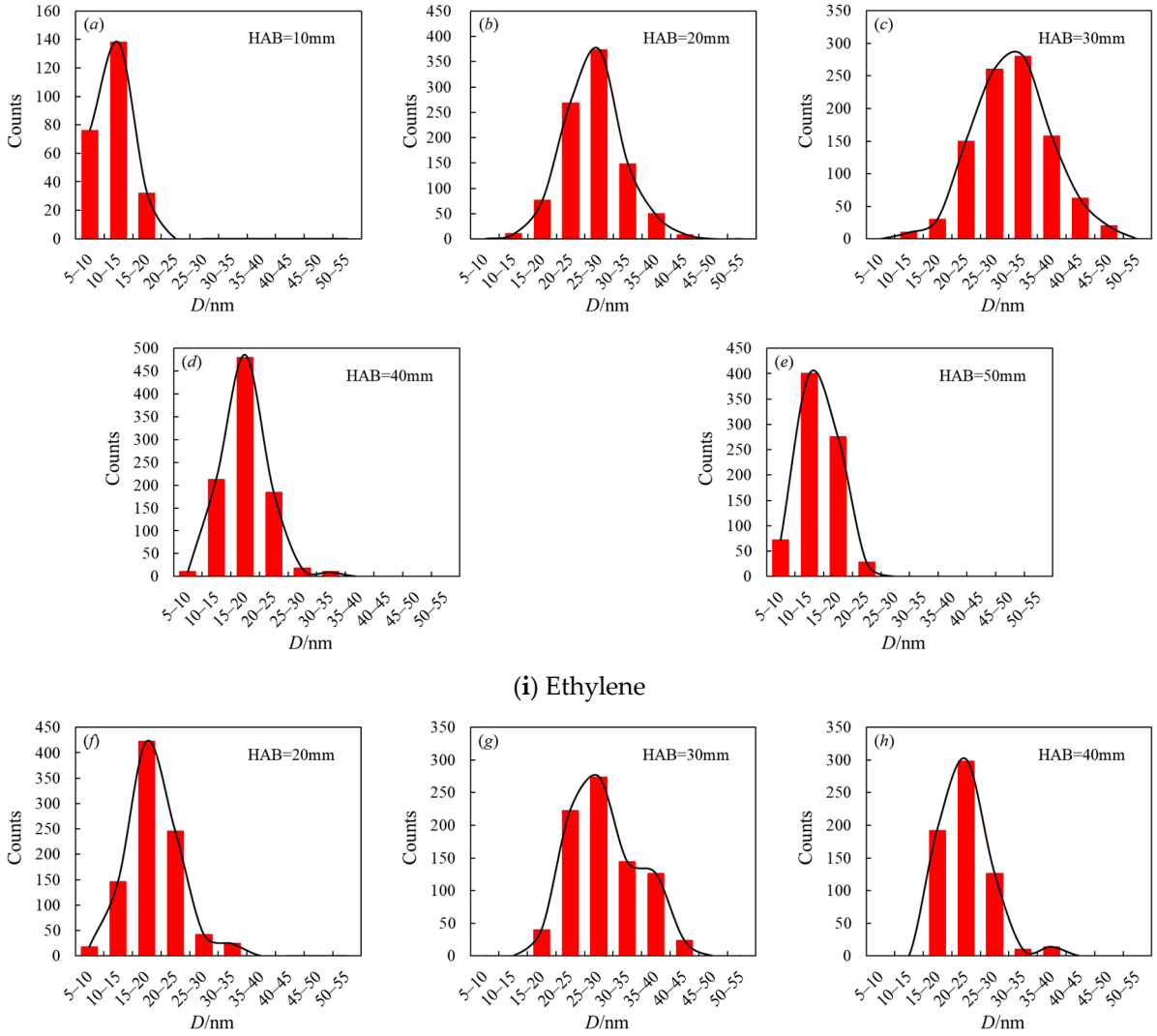

Figure 5. The particle size distribution of primary soot particles at different flame heights for ethylene and ethane flames.

Figure 6 compares D_p at different flame heights for the ethylene and ethane flames. As Figure 6 shows, D_p in the ethylene and ethane flames increases and then decreases as they grow in height, reaching the maximum values when the HAB = 30 mm, at 30.7 nm and 28.6 nm, respectively. This trend is caused by the laminar diffusion flame structure, which can be divided into an inner flame surface and an outer flame surface, with combustion mainly occuring between these two surfaces [37].

In addition, at an HAB = 10 mm, there is a delay in the production of soot particles from the ethane flame compared to that from the ethylene flame. A small number of chain-like soot particle aggregations are observed in the ethylene flame sample, while only unformed carbon nuclei are observed in the ethane flame sample. This is because it mainly comprises the gas-phase chemical reaction zone and the soot nucleation zone at this position [38]. However, ethylene has a lower ignition point than ethane, with easily breakable carbon double bonds, making the combustion reaction rate of ethylene greater than that of ethane. Given this, soot particles ultimately form at a higher rate in the ethylene flame than in the ethane flame.

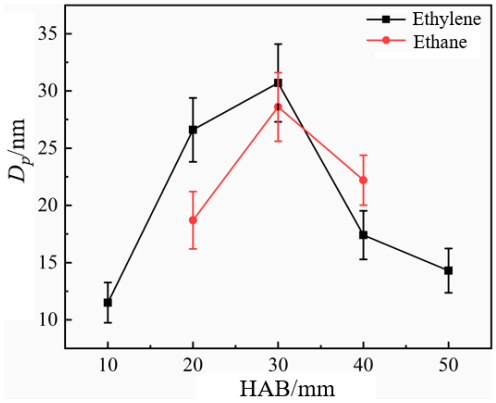

Figure 6. Change in D_p with different HABs at an oxygen concentration of 21%.

Meanwhile, at the highest positions of the flame (HAB = 50 mm and 60 mm), the flame width narrows, the gas flow rate speeds up, and the intrusive sampling method has a greater impact on the flame's structure, resulting in the sampling position deviating from the center of the flame axis. Consequently, complete soot particles cannot be collected on the carbon film for the purpose of calculating the fractal dimension statistics.

The changes in D_f with HAB for the ethylene and ethane flames are depicted in Figure 7, where it is evident that D_f increases with an increase in the HAB. The D_f of the soot particles in the ethylene flame rises from 1.33 at an HAB = 20 mm to 1.94 at an HAB = 50 mm, while the D_f of the soot particles in the ethane flame increases from 1.77 at an HAB = 20 mm to 1.88 at an HAB = 40 mm. At identical HABs, the D_f of the soot particles in the ethylene flame is consistently smaller than that in the ethane flame.

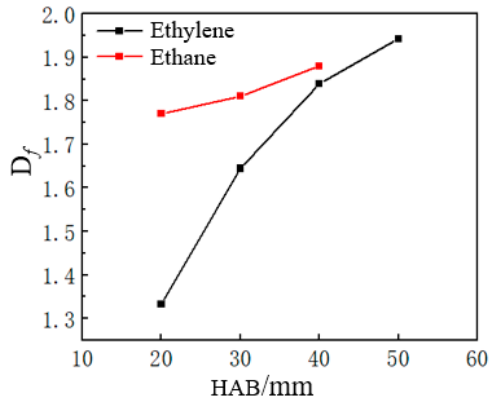

Figure 7. Change in D_f with HAB at an oxygen concentration of 21%.

The variation in the fractal dimension can be explained according to Figure 4. The variation of D_f in the ethylene flame is such that at an HAB = 20 mm, most of the soot particles in the flame are chain-like agglomerates, and D_f is 1.33. As the flame height increases, the flame becomes brighter and the temperature increases, with the most intense brightness and temperature observed at an HAB = 30~40 mm. This also corresponds to the location with the highest soot particle concentration [39]. The morphologies of the soot particles change from being chain-like to ring-like, and D_f increases. As the flame height increases further (HAB = 50 mm), soot particles are more likely to collide, condense, and aggregate, and the primary soot particles accumulate over a large area. The soot particles gradually change from being ring-like to forming denser, fibrous network structures, leading to an increased D_f value of 1.94. For the soot particles in the ethane flame, as the flame height increases (HAB = 40 mm), agglomerates overlap more, leading to a further increase in D_f to 1.88.

4. Soot Particle Morphologies and Nanostructures at Different Oxygen Concentrations

4.1. Soot Particle Morphologies at Different Oxygen Concentrations

The effects of oxygen concentration on soot particle morphology and nanostructure are investigated by adjusting the air and oxygen flow rates. As the primary soot particles in the brightest area of the flame are mature structures, and are easy to observe, the soot particles in the ethylene and ethane flames are sampled and observed at different oxygen concentrations at an HAB = 30 mm, as shown in Figure 8. Increasing the oxygen concentration is found to intensify the agglomeration, and the aggregates exhibit a cluster or network structure. Comparing the morphologies of the soot particles in the ethylene and ethane flames, at the same oxygen concentration, it is observed that the degree of agglomeration of the soot particles is greater in the ethane flame than in the ethylene flame. This may be attributed to the high temperature in the ethylene flame, inhibiting the generation of soot precursors.

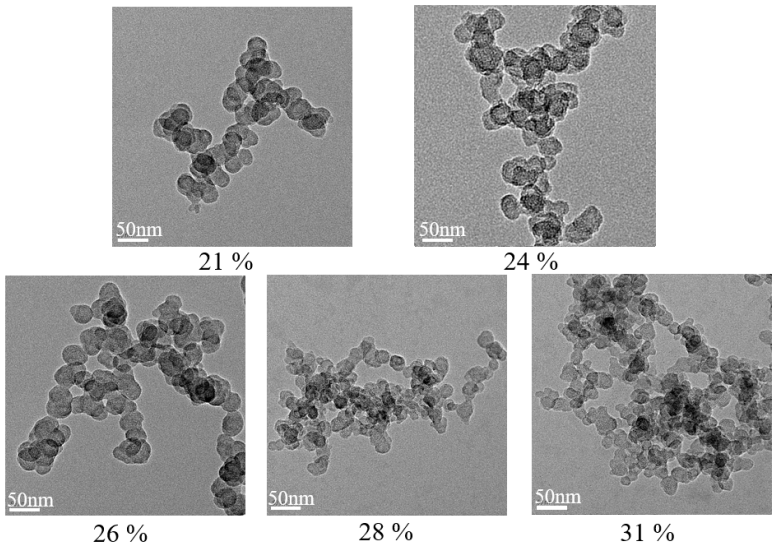

(**a**) Ethylene

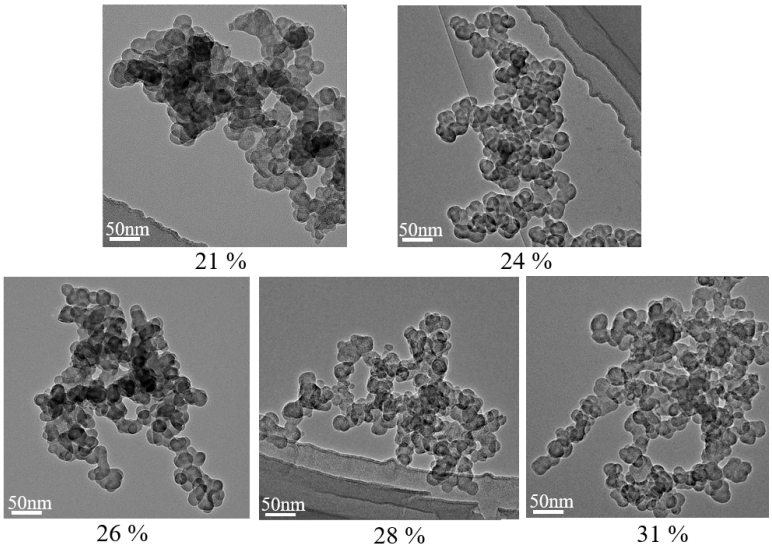

(**b**) Ethane

Figure 8. Soot particle morphologies at different oxygen concentrations at an HAB = 30 mm.

4.2. D_p and D_f at Different Oxygen Concentrations

In order to quantitatively compare the influence of oxygen concentration on soot particle morphologies, the changes in D_p and D_f at an HAB of 30 mm in the ethylene and ethane flames at different oxygen concentrations were analyzed, as shown in Figure 9. It can be seen from Figure 9 that D_p in the ethylene flame decreases from 30.7 nm to 18.3 nm with an increase in the oxygen concentration, while in the ethane flame, it decreases from 28.6 nm to 22.5 nm, corresponding to 40.4% and 21.3%, respectively. This concurs with the results obtained by Kwang [13]. This is explained by the increase in the oxygen concentration increasing the diffusion rate of oxygen and enhancing the surface oxidation of the primary soot particles, leading to a decrease in D_p.

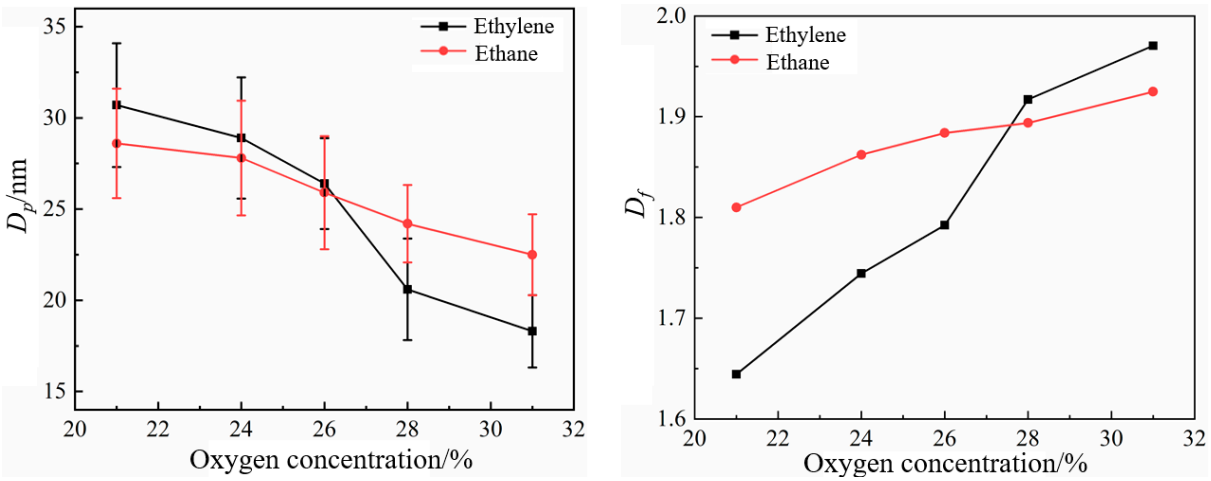

Figure 9. D_p and D_f in the ethylene and ethane flames at different oxygen concentrations.

As shown in Figure 9, as the oxygen concentration increases from 21% to 31%, D_f in the ethylene flame increases from 1.64 to 1.97, an increase of 20.1%, while in the ethane flame, it increases from 1.81 to 1.92, an increase of 6.1%. This trend is consistent with the trend obtained by Verma [40]. This is because with an increase in the oxygen concentration, the combustion reaction intensifies; the flame narrows; soot particles move faster within the flame, which increases the probability of collision and agglomeration; the fractal dimensions of the soot particles resultantly increase; and, finally, denser network aggregates are formed. D_f increases more in the ethylene flame than in the ethane flame, because unsaturated bond reactions occur faster in ethylene, and more oxygen in unit time is required, so the oxygen concentration has a greater impact on the D_f in the ethylene flame.

4.3. The Nanostructure of Primary Soot Particles at Different Oxygen Concentrations

The HRTEM images of the primary soot particles, at an HAB = 30 mm, were magnified 500,000 times in order to investigate the influence of oxygen concentration on the nanostructure of primary soot particles, as illustrated in Figures 10 and 11. As can be seen from Figures 10 and 11, the primary soot particles at an HAB = 30 mm exhibit maturity, characterized by a typical core-shell structure, wherein a carbon layer is concentrically arranged around a carbon core. The flame temperature increases with the rise in the oxygen concentration, while the carbon layer exhibits a highly stable concentric configuration.

In order to quantitatively compare the effects of different oxygen concentrations on the nanostructure of primary soot particles, the T_f and D_s of the primary soot particles at this location were analyzed and counted, as shown in Figures 12 and 13, respectively.

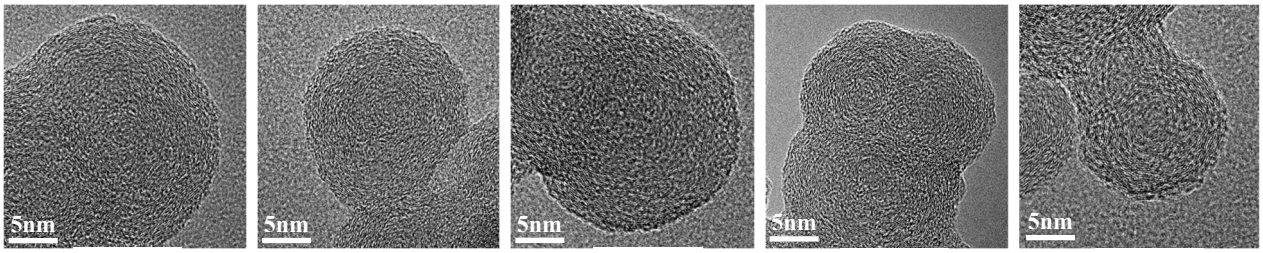

(**a**) 21% (**b**) 24% (**c**) 26% (**d**) 28% (**e**) 31%

Figure 10. Soot particle nanostructures at different oxygen concentrations at an HAB = 30 mm in the ethylene flame.

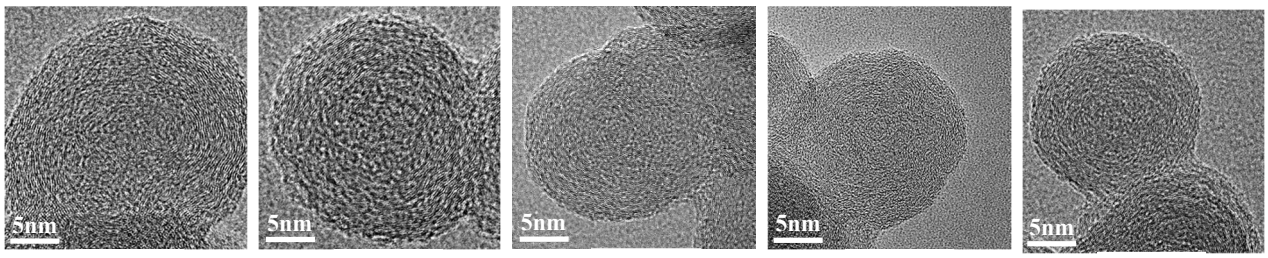

(**a**) 21% (**b**) 24% (**c**) 26% (**d**) 28% (**e**) 31%

Figure 11. Soot particle nanostructures at different oxygen concentrations at an HAB = 30 mm in the ethane flame.

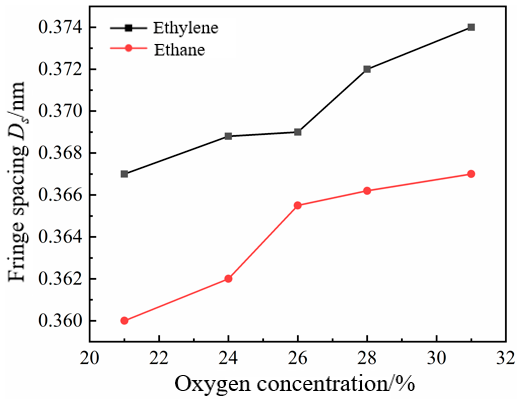

Figure 12. D_s in the ethylene and ethane flames at different oxygen concentrations.

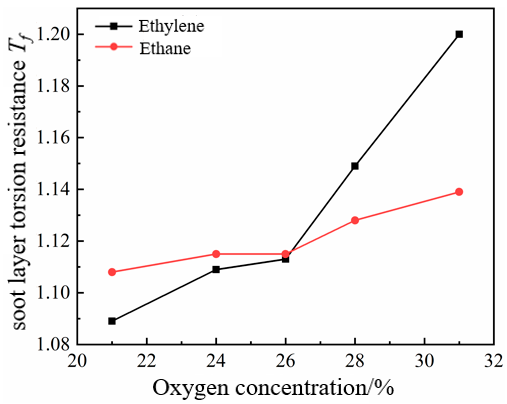

Figure 13. T_f in the ethylene and ethane flames at different oxygen concentrations.

Figure 12 shows that D_s increases as the oxygen concentration increases from 21% to 31%. Specifically, the D_s in the ethylene flame increases from 0.367 nm to 0.374 nm, while the D_s in the ethane flame increases from 0.36 nm to 0.367 nm. An increase in the oxygen concentration reduces the temperature and energy required for soot particle oxidation [41]. Consequently, a higher oxygen concentration increases the surface oxidation activity on the soot particles, resulting in the oxidation of the outer carbon layer of numerous mature soot particles [42]. This alteration causes a shift in the carbon layer from a parallel arrangement to a curved arrangement, ultimately leading to larger D_s values and a looser soot particle structure.

Figure 13 shows the changes in T_f in the ethylene and ethane flames with the oxygen concentration. Specifically, the T_f in the ethylene flame increases from 1.089 to 1.2, while the T_f in the ethane flame increases from 1.108 to 1.139. On the one hand, as the oxygen concentration increases, the outer carbon layer becomes more susceptible to oxidation, resulting in a decrease in both the soot particle size and the length of the carbon layer. On the other hand, with an elevated oxygen concentration, the combustion reaction intensifies, leading to a reduction in the flame height and a shorter residence time for soot particles within the flame. The duration of soot particle residence significantly impacts graphitization [34], whereby a shorter residence time corresponds the soot particles having a more disordered structure and an increased T_f.

5. Conclusions

Soot particles were sampled at different HABs from ethylene and ethane flames, and morphologies and nanostructures of the soot particles were observed using HRTEM to study their growth in a coaxial laminar diffusion flame and to analyze the effects of double bonds on the structures of soot particles. The conclusions are as follows:

(1) At an oxygen concentration of 21%, ethylene laminar flames are taller and brighter due to the presence of double bonds in ethylene. The ethylene laminar flame was 64.34 mm tall, while ethane was 52.11 mm tall.

(2) As the oxygen concentration increases from 21% to 31%, the ethylene and ethane flames gradually become less tall and brighter, as the increase in oxygen accelerates the fuels' chemical reaction.

(3) At the same oxygen concentration, the D_p of the primary soot particles along the flame axis shows a trend of first increasing and then decreasing. At an HAB = 25–30 mm, D_p is the largest. The D_f of the soot particles increases with an increase in the flame height, and the morphologies of the soot particles evolve from strips and chains into clusters.

(4) At the same flame height (HAB = 30 mm), with an increase in the oxygen concentration, the D_p of the primary soot particles decreases, the D_f of the soot particles increases, and the soot particles aggregate more densely. This is because the flame height decreases with an increase in the oxygen concentration, which means the soot particles are sampled at a position closer to the region where a high concentration of soot particles is generated.

(5) At the same flame height (HAB = 30 mm), the higher the oxygen concentration, the higher the oxidation activity, and the D_s and T_f of the primary soot particles increase; this causes the primary soot particles to become looser, and the carbon layer changes from a parallel arrangement to a curved arrangement.

Author Contributions: Conceptualization, H.J. and D.Z.; methodology, H.J.; software, R.Z.; validation, D.Z.; writing—original draft preparation, R.Z.; writing—review and editing, H.J. and Z.W.; supervision, H.J.; project administration, P.D.; funding acquisition, H.J. and P.D. All authors have read and agreed to the published version of the manuscript.

Funding: This research was supported by the National Natural Science Foundation of China, grant number 51706163.

Data Availability Statement: The data presented in this study are available on request from the corresponding author.

Conflicts of Interest: The authors declare no conflicts of interest. The funders had no role in the design of the study; in the collection, analyses, or interpretation of the data; in the writing of the manuscript, or in the decision to publish the results.

References

1. Bond, T.C.; Doherty, S.J.; Fahey, D.W.; Forster, P.M.; Berntsen, T.; DeAngelo, B.J.; Flanner, M.G.; Ghan, S.; Kärcher, B.; Koch, D.; et al. Bounding the role of black carbon in the climate system: A scientific assessment. *J. Geophys. Res. Atmos.* **2013**, *118*, 5380–5552. [CrossRef]
2. Murray, J.T. Modeling soot formation in flames and Reactors: Recent progress and current challenges. *Proc. Combust. Inst.* **2023**, *39*, 805–823.
3. He, Z.; Dan, Z.; Dakun, S.; Bernhard, S. Electrical power, energy efficiency, NO and CO emissions investigations of an ammonia/methane-fueled micro-thermal photovoltaic system with a reduced chemical reaction mechanism. *Energy* **2024**, *305*, 132248.
4. Haifeng, L.; Jeffrey, D.A.; Yang, Z.; Xingyu, S.; Linxun, X.; Xueli, J.; Shuaishuai, W. A perspective on the overarching role of hydrocarbon, ammonia, and methanol carbon-neutral fuels towards net zero emission in the next three decades. *Energies* **2023**, *16*, 280.
5. Muhammad, K.; Philippe, G.; Jérôme, B.; Guillaume, L. Sooting tendencies of primary reference fuels in atmospheric laminar diffusion flames burning into vitiated air. *Combust. Flame* **2014**, *161*, 1575–1586.
6. Puneet, V.; Mohammad, J.; Ali, Z.; Edmund, P.; Yi, G.; Chiemeriwo, G.O.; Svetlana, S.; Richard, B.; Zoran, R. Soot particle morphology and nanostructure with oxygenated fuels: A comparative study into cold-start and hot-start operation. *Environ. Pollut.* **2021**, *275*, 116592.
7. Yu, W.; Suk, H.C. Soot formation in laminar counterflow flames. *Prog. Energy Combust. Sci.* **2019**, *74*, 152–238.
8. Ahmed, H.A.; Ashraf, M.A.; Steinmetz, S.A.; Dunn, M.J.; Masri, A.R. The role of DME addition on the evolution of soot and soot precursors in laminar ethylene jet flames. *Proc. Combust. Inst.* **2021**, *38*, 5319–5329. [CrossRef]
9. Penelope, M.; Hai, W.; Michael, F. A computational study of sooting limits in laminar premixed flames of ethane, ethylene, and acetylene. *Combust. Flame* **1993**, *93*, 467–482.
10. Qiu, L.; Hua, Y.; Zhuang, Y.; Wei, J.; Qian, Y.; Cheng, X. Numerical investigation into the decoupling effects of hydrogen blending on flame structure and soot formation in a laminar ethylene diffusion flame. *Int. J. Hydrogen Energy* **2020**, *45*, 15672–15682. [CrossRef]
11. Xu, L.; Yan, F.; Wang, Y.; Chung, S.H. Chemical effects of hydrogen addition on soot formation in counterflow diffusion flames: Dependence on fuel type and oxidizer composition. *Combust. Flame* **2020**, *213*, 14–25. [CrossRef]
12. Ashraf, M.A.; Ahmed, H.A.; Steinmetz, S.; Dunn, M.J.; Masri, A.R. On the effects of varying coflow oxygen on soot and precursor nanoparticles in ethylene laminar diffusion flames. *Fuel.* **2021**, *300*, 120913. [CrossRef]
13. Wang, Q.; Legros, G.; Bonnety, J.; Morin, C.; Matynia, A.; Consalvi, J.L.; Liu, F. Experimental assessment of the sudden-reversal of the oxygen dilution effect on soot production in coflow ethylene flames. *Combust. Flame* **2017**, *183*, 242–252. [CrossRef]
14. Karataş, A.E.; Gigone, B.; Gülder, Ö.L. Soot aggregate morphology deduced from thermophoretic sampling in coflow laminar methane diffusion flames at pressures up to 30 bar. *Combust. Flame* **2020**, *222*, 411–422. [CrossRef]
15. Li, J.; Gan, Z.; Liang, Y. An experimental investigation of soot morphology and nanostructure in high-pressure co-flow laminar methane diffusion flames. *Exp. Therm. Fluid Sci.* **2022**, *136*, 110676. [CrossRef]
16. Hafiz, M.F.A.; William, L.R. Investigating soot parameters in an ethane/air counterflow diffusion flame at elevated pressures. *Combust. Sci. Technol.* **2021**, *193*, 1827–1842.
17. Chu, H.; Han, W.; Cao, W.; Gu, M.; Xu, G. Effect of methane addition to ethylene on the morphology and size distribution of soot in a laminar co-flow diffusion flame. *Energy* **2019**, *166*, 392–400. [CrossRef]
18. Feng, S.; Hong, R.; Qi, J.; Dong, W.; Qiu, B.; Yan, X.; Chu, H. Effect of NH_3 addition on soot morphology and nanostructure evolution in laminar ethylene diffusion flame. *Fuel* **2023**, *350*, 128845. [CrossRef]
19. Liu, Q.; Sun, J.; Li, S.; Zhang, F.; Gu, M.; Wang, Y. Study of soot microscopic characteristics in hydrogen/methane/ethylene co-flow diffusion flame. *Energy* **2024**, *290*, 130091. [CrossRef]
20. Bönig, M.; Feldermann, C.; Jander, H.; Lüers, B.; Rudolph, G.; Wagner, H.G. Soot formation in premixed C_2H_4 flat flames at elevated pressure. *Proc. Combust. Inst.* **1991**, *32*, 1581–1587. [CrossRef]
21. Bockhrom, H. Soot formation in combustion: Mechanisms and models. *Life Support Syst. J. Eur. Soc. Artif. Organs* **1995**, *3*, 727–744.
22. Oh, K.C.; Shin, H.D. The effect of oxygen and carbon dioxide concentration on soot formation in non-premixed flames. *Fuel* **2006**, *85*, 615–624. [CrossRef]
23. Liu, C.; Zhu, L.; Gao, Z.; Li, H.; Huang, Z. Effects of molecular O_2 and NO_2 on particle size distribution, morphology and nanostructure of diffusion flame soot oxidized in a flow reactor. *Fuel* **2018**, *234*, 335–346. [CrossRef]
24. Escudero, F.; Fuentes, A.; Demarco, R.; Consalvi, J.L.; Liu, F.; Elicer-Cortés, J.C.; Fernandez-Pello, C. Effects of oxygen index on soot production and temperature in an ethylene inverse diffusion flame. *Exp. Therm. Fluid Sci.* **2016**, *73*, 101–108. [CrossRef]
25. Marek, S.; Ahmet, E.K. Effects of oxygen on soot formation in laminar co-flow flames of binary mixtures of ethane, DME, and oxygen. *Combust. Flame* **2021**, *229*, 111413.

26. Katsufumi, K.; Tetsuya, A.; Sanghoon, K.; Lyle, P. Uncertainty in Sampling and TEM Analysis of Soot Particles in Diesel Spray Flame. *SAE Paper* **2013**. [CrossRef]
27. Brasil, A.M.; Farias, T.L.; Carvalho, M.G. A recipe for image characterization of fractal-like aggregates. *J. Aerosol Sci.* **1999**, *30*, 1379–1389. [CrossRef]
28. Wei, J.; Zeng, Y.; Pan, M.; Zhuang, Y.; Qiu, L.; Zhou, T.; Liu, Y. Morphology analysis of soot particles from a modern diesel engine fueled with different types of oxygenated fuels. *Fuel* **2020**, *267*, 117248. [CrossRef]
29. Wang, T.; Qiao, X.; Li, T.; Zhao, P.; Zhao, K.; Wu, G. Micro-nano morphology parameters and mechanical properties of soot particles sampled from high pressure jet flames of diesel from direct coal liquefaction. *Fuel* **2023**, *332*, 126084. [CrossRef]
30. Huaqiang, C.; Weiwei, H.; Wenjian, C.; Changfa, T.; Mohsin, R.; Longfei, C. Experimental analysis of effect of oxygen concentration on soot formation in ethylene diffusion flame. *J. Energy Inst.* **2019**, *92*, 1294–1302.
31. Yang, S.; Lu, S.; Cheng, X.; Zheng, R.; Yuen, R.K.K. Smoke production and fractal structure properties of soot from n-Heptane pool fires under low pressures. *Fire Technol.* **2016**, *52*, 1915–1937. [CrossRef]
32. Snelling, D.R.; Liu, F.; Smallwood, G.J.; Gülder, Ö.L. Determination of the soot absorption function and thermal accommodation coefficient using low-fluence LII in a laminar coflow ethylene diffusion flame. *Combust. Flame* **2004**, *136*, 180–190. [CrossRef]
33. Mei, J.; Wang, M.; Hou, D.; Tang, Q.; You, X. Comparative study on nascent soot formation characteristic in laminar premixed acetylene, ethylene, and ethane flames. *Energy Fuels* **2018**, *32*, 11683–11693. [CrossRef]
34. Liu, Y.; Xu, Y.; Zhang, K.; Zhang, P.; Cheng, X. Effects of ammonia addition on soot formation in ethylene laminar diffusion flames. Part 3. The morphology and nanostructure of soot particles. *Fuel* **2023**, *332*, 126082. [CrossRef]
35. Li, Z.; Qiu, L.; Cheng, X.; Li, Y.; Wu, H. The evolution of soot morphology and nanostructure in laminar diffusion flame of surrogate fuels for diesel. *Fuel* **2018**, *211*, 517–528. [CrossRef]
36. Köylü, Ü.Ö.; Mcenally, C.S.; Rosner, D.E.; Pfefferle, L.D. Simultaneous Measurements of Soot Volume Fraction and Particle Size/Microstructure in Flames Using a Thermophoretic Sampling Technique. *Combust. Flame* **1997**, *110*, 494–507. [CrossRef]
37. Bowen, L.; Chengjing, W.; Yindi, Z.; Bing, L.; Fanjin, Z.; Takyi, S.A.; Tontiwachwuthikuld, P. Effect of CO_2/H_2O addition on laminar diffusion flame structure and soot formation of oxygen-enriched ethylene. *J. Energy Inst.* **2022**, *102*, 160–175. [CrossRef]
38. Karatas, A.E. *Soot Formation in Co-Flow and Counterflow Laminar Diffusion Flames of Fuel Mixtures*; University of Toronto: Toronto, ON, Canada, 2009.
39. Khanehzar, A.; Cepeda, F.; Dworkin, S.B. The influence of nitrogen and hydrogen addition/dilution on soot formation in coflow ethylene/air diffusion flames. *Fuel* **2022**, *309*, 122244. [CrossRef]
40. Puneet, V.; Mohammad, J.; Rahman, S.M.A.; Edmund, P.; Svetlana, S.; Ashley, D.; Richard, B.; Zoran, R. The impact of chemical composition of oxygenated fuels on morphology and nanostructure of soot particles. *Fuel* **2020**, *259*, 116167.
41. Ziye, W.; Ye, L.; Gang, L.; Chonglin, S.; Yuan, B. The influence of fuel air equivalence ratio on soot nano structure, fractal dimension and oxidation activity in ethylene premixed flame. *J. Combust. Sci. Technol.* **2020**, *26*, 280–286.
42. Hurt, R.H.; Crawford, G.P.; Shim, H.S. Equilibrium nanostructure of primary soot particles. *Proc. Combust. Inst.* **2000**, *28*, 2539–2546. [CrossRef]